International Journal of Engineering and Information Systems (IJEAIS)
ISSN: 2000-000X
Vol. 1 Issue 9, November – 2017, Pages: 129-142

Numerical Analysis of Enhanced Heat Transfer in the Metal Foam System Filled with Phase Change Materials

Hui Wang[1], Qing-Hua Qin[2]
[1]College of Civil Engineering & Architecture, Henan University of Technology
Zhengzhou, China
[2]Research School of Engineering, Australian National University
Canberra, Australia
Email: [1]Huiwang_china@163.com, [2]Qinghua.qin@anu.edu.au

Abstract*—The melting efficiency is often limited by the low thermal conductivity of PCMs. In this paper, numerical simulation is carried out for analyzing the enhanced heat transfer in the metal honeycomb foam system filled with PCMs. In the present PCM/FOAM model, octadecane is used as PCM, and the metal honeycomb foam with 96% porosity is employed as enhancer to improve the heat transfer performance in the PCM and accelerate its melting. The PCM/FOAM model is heated on one of surfaces with a constant heat flux so that the PCM can be heated from the solid state to the pure liquid state. The enhanced heat transfer in the PCM/FOAM model is numerically solved by the finite element technique. The numerical results obtained are compared with those for the pure PCM to illustrate the enhancing effect due to the presence of metal foam. Results show that the overall heat transfer rate can be increased by about 100% due to the addition of metal foam. Finally, the comparative analysis is carried out for different metal matrix materials and PCMs.*

Keywords— Metal foam; Phase change material; heat transfer; finite element.

1. INTRODUCTION

Phase change materials such as octadecane, paraffin wax, hydrated salts, and acids, exhibit a high enthalpy of fusion in a relatively small volume, so that they can been applied for thermal energy storage by using their excellent capacity of latent heat of fusion, that is, storing and releasing large amount of heat energy during melting and solidification [1,2]. However, the energy storage capacity is often limited by the intrinsic defect of low thermal conductivity of PCMs, as a result the thermal energy from the outer environment is difficult to transfer into the solid PCMs to make them melt quickly. Further, the stored thermal energy in the liquid PCMs is also difficult to release for making them solidify in a short time. The overall storing and releasing period of the PCMs is usually time-consuming and the efficiency of thermal energy storage is relatively low.

In order to improve the heat transfer rate in PCMs, extensive studies have been carried out by adding materials with higher thermal conductivity in the system. So far, the commonly used enhancers include the metal powder, metal foam and graphite. For example, Mettawee and Assassa formed a latent heat storage system by placing aluminium powder into the paraffin wax. The reported results showed that the heat transfer performance of the PCM-aluminium composite material was improved as compared to the case of pure paraffin wax [3]. Martin et al. studied the heat transfer performance of paraffin-graphite composites [4]. Sarı and Karaipekli investigated the influence of expanded graphite (EG) addition on the thermal conductivity of the paraffin/EG composites [5]. Ji et al. revealed that the addition of ultrathin-graphite foams in a PCM can increase the thermal conductivity of PCM by up to 1800%, with negligible change in the PCM melting temperature or mass specific heat of fusion [6]. Li et al. designed a sandwiched cooling structure using copper metal foam saturated with phase change materials and studied experimentally and numerically the thermal efficiency of the composite system [7,8]. Zhao et al. studied the enhanced heat transfer behavior in the paraffin wax PCM embedded in open-cell copper foam [9]. In the studies reviewed above, both experimental and numerical methods are extensively used for analyzing the enhanced heat transfer in the composite systems consisting of PCMs and enhanced materials. Compared to the experimental method, the numerical simulation can provide more flexible and economic ways for the analysis of the complicated enhanced PCM system.

In this paper, the melting procedure of phase change material, octadecane used here, in the metal honeycomb foam (FOAM for short hereafter) is numerically investigated to examine the enhanced heat transfer capability of phase change materials by introducing the regular metal foam. In addition, the influence of thermal conductivity of metal matrix material on the melting efficiency of the PCM is studied for different matrix materials and PCMs.

The paper is organized as follows. Section 2 briefly describes the physical and mathematical model of transient heat transfer in the PCM/FOAM system, and related numerical results are given in Section 3. Finally, some conclusions are summarized in Section 4.

2. TRANSIENT HEAT TRANSFER MODEL IN THE PCM/FOAM SYSTEM

Consider a practical trimmed honeycomb foam structure made of metal aluminium as shown in Figure 1. The length and width of the foam model are 196.1576mm and 56.6258mm, respectively. For each cell, the side length is 3.7mm and the wall thickness is 0.13mm. The porosity of the foam is, therefore, 96%. The metal foam is filled with octadecane [10]. The thermophysical properties of metal aluminium [11] and octadecane [10] are listed in Table 1 for reference.

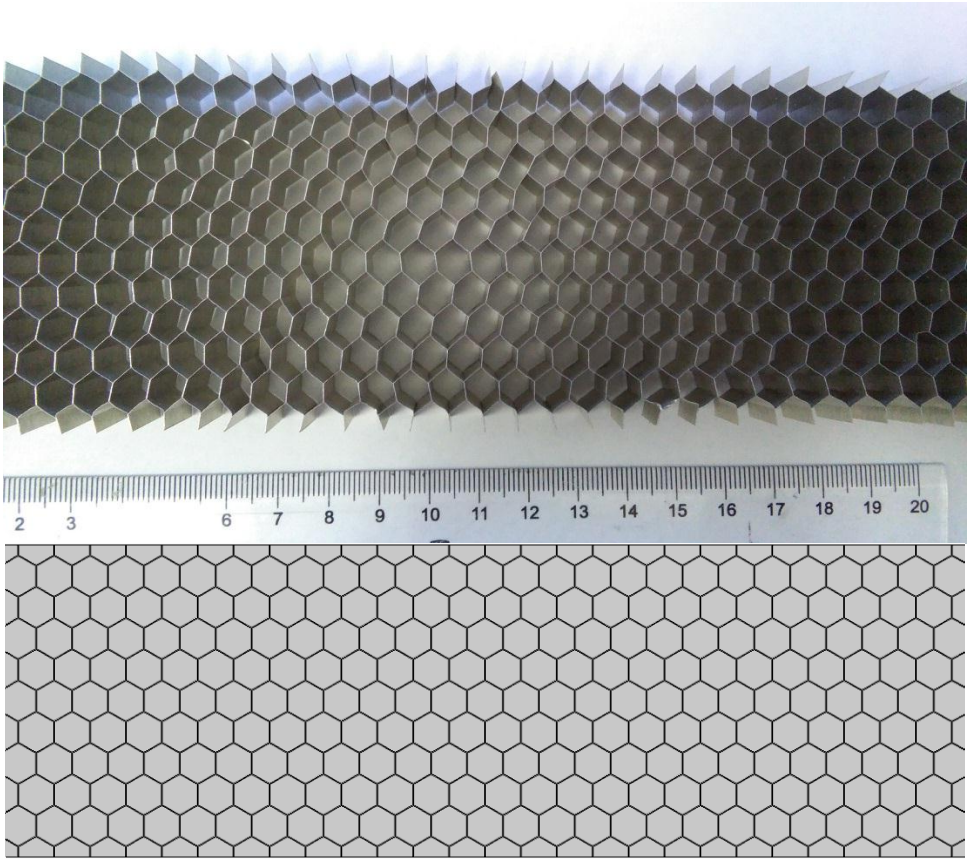

Figure 1: Actual honeycomb foam (above) and the 2D geometrical model (bottom)

Table 1. Thermophysical properties of octadecane and aluminium

Property	Octadecane	Aluminium
Density ρ (kg/m^3)	800	2675
Mass heat capacity c_p $(J/kg/K)$	1250	903
Latent heat of fusion L_f (J/kg)	125000	/
Melting temperature T_m (K)	303	/
Thermal conductivity k $(W/m/K)$	0.2	211

It's assumed that there is an energy input G (Wm-2) from the bottom of the model system consisting of metal foam and octadecane. The other surfaces are covered with insulation material, as shown in Figure 2. Obviously, the incident energy G is transferred into the middle region of the system to force octadecane changing its phase from solid to liquid.

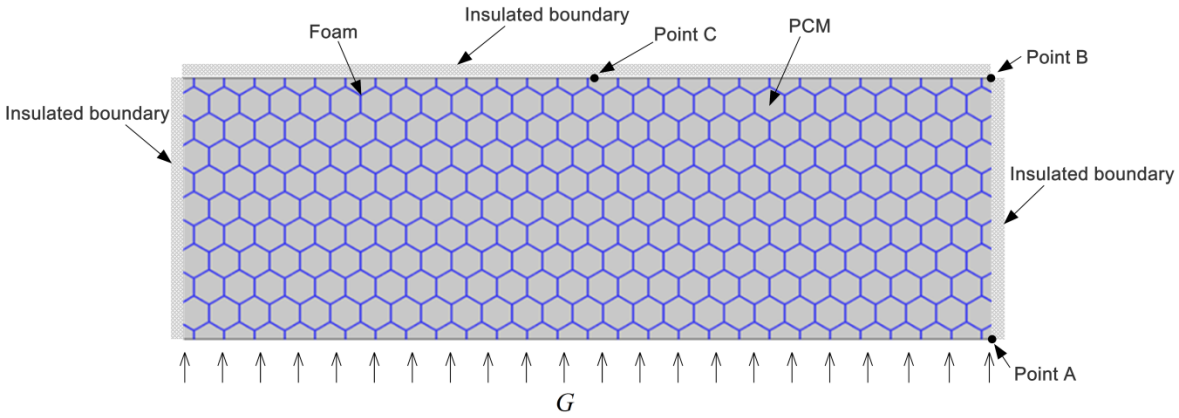

Figure 2. Boundary conditions of the PCM/FOAM system

For the heat transfer in the PCM/FOAM system, the natural convection in the PCM liquid phase caused by the fluid flow driven by buoyancy force is not taken into consideration due to the small size and the closed-cell feature of the pores [9]. Only the heat conduction in the solid metal foam phase, solid PCM and liquid PCM is considered. According to heat conduction theory [11], the transient heat conduction equation in material coordinates is written as

$$\rho_e c_{pe} \frac{\partial T(\mathbf{x},t)}{\partial t} = \nabla \cdot [k_e \nabla T(\mathbf{x},t)] + Q \tag{1}$$

where $\rho_e(\mathrm{kgm^{-3}})$, $c_{pe}(\mathrm{Jkg^{-1}K^{-1}})$, $k_e(\mathrm{Wm^{-1}K^{-1}})$ are effective material density, mass heat capacity at constant pressure, and thermal conductivity, respectively. $T(\mathrm{K})$ is the temperature, and $Q(\mathrm{Wm^{-3}})$ is an interior heat source per unit volume. In this study, the interior heat source is set to be zero.

For the metal foam material, the effective material properties can be given by

$$\rho_e = \rho_m, \quad c_{pe} = c_{pm}, \quad k_e = k_m \tag{2}$$

where the subscript *m* stands for the solid metal material of foam. For aluminium material, the thermo-property values can be found in Table 1.

While, for the PCM, there is phase change from the PCM solid phase to the PCM liquid phase when the actual temperature reaches its melting temperature T_m. During the melting process, the large latent heat of fusion is absorbed. Actually, the phase change usually takes place within a temperature interval, and the latent heat can be introduced into an apparent heat capacity during phase change. Thus, the effective material properties should be modified as

$$\rho_e = \begin{cases} \rho_s, & T < T_s \\ \dfrac{\rho_s + \rho_l}{2}, & T_s < T < T_l \\ \rho_l, & T > T_l \end{cases} \tag{3}$$

$$c_{pe} = \begin{cases} c_{ps}, & T < T_s \\ \dfrac{c_{ps} + c_{pl}}{2} + \dfrac{L_f}{\Delta T}, & T_s < T < T_l \\ c_{pl}, & T > T_l \end{cases} \tag{4}$$

$$k_e = \begin{cases} k_s, & T < T_s \\ \dfrac{k_s + k_l}{2}, & T_s < T < T_l \\ k_l, & T < T_l \end{cases} \tag{5}$$

where the subscripts s and l stand for the solid and liquid phases of PCM, respectively. For the specific single melting temperature T_m, we can set $T_s = T_m - \Delta T/2$ and $T_l = T_m + \Delta T/2$, with the introduced phase change temperature interval ΔT. In this study, we set the phase change temperature interval $\Delta T = 1K$. Due to the minor difference of these parameter values for the solid and liquid states, in the following computation, it's assumed that the thermophysical properties of solid and liquid phases of PCM are same and keep constant in the simulation. For Octadecane PCM, the values of these parameters are given in Table 1 for reference.

Besides, the initial condition and the boundary conditions should be applied to make the problem solvable. At the initial instance $t = 0$, the PCM/FOAM system is assumed to be with the temperature T_0. The initial temperature condition is, then, written as

$$T(\mathbf{x}, t = 0) = T_0 \tag{6}$$

In the analysis, it's assumed that the bottom surface of the PCM/FOAM system is subjected to an inward heat flux G and the remaining surfaces are insulted. Hence, the boundary conditions for $t > 0$ are written as

$$\begin{aligned} \mathbf{n} \cdot \mathbf{q} &= -G \quad \text{on the bottom surface} \\ \mathbf{n} \cdot \mathbf{q} &= 0 \quad \text{on other surfaces} \end{aligned} \tag{7}$$

where $\mathbf{n}$ is the normal vector of the surface and $\mathbf{q}$ is the heat flux vector per unit area ($\mathrm{Wm^{-2}}$) expressed by the Fourier law

$$\mathbf{q} = -k_e \nabla T \tag{8}$$

The boundary conditions of the PCM/FOAM system are tabulated in Table 2.

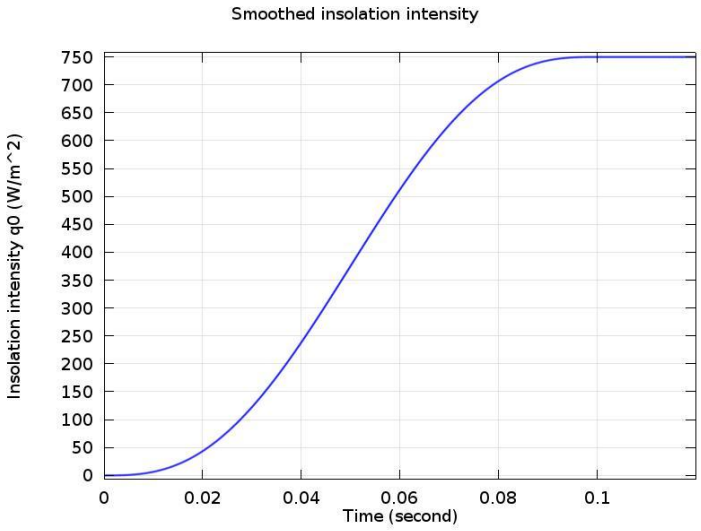

Figure 3: Smoothed incident energy intensity G

Table 2. Boundary conditions of the PCM/FOAM system

Quantity	Value
Initial temperature T_0 (K)	293
Incident energy intensity G ($\mathrm{Wm^{-2}}$)	750

In the practical simulation, the incident energy intensity, i.e. $G = 750\ \mathrm{Wm^{-2}}$, is applied over the bottom surface of the system since $t > 0$. Clearly, it will induce a sudden temperature change at the starting time. To bypass this problem, a smoothed function which increases the incident energy intensity from 0 to 750 $\mathrm{Wm^{-2}}$ within 0.1s is introduced, as shown in Figure 3.

3. NUMERICAL RESULTS AND DISCUSS

In this section, the enhanced heat transfer in the PCM/FOAM system is numerically investigated. Apart from analytical solutions which are available only for a few problems with simple geometries and boundary conditions [12-16], numerical methods such as finite element method [17,18], finite difference method [9,19,20], and the boundary element method [21] can be used to solve such a complex problem. Among them, the finite element method based on the element-level approximation and the virtual work principle is very suitable for such coupling heat transfer involving solid phase and fluid phase. In this study, the finite element analysis is performed using COMSOL multiphysics, and the free triangular elements are used for both the solid metal wall and the PCM. Additionally, in order to show the effect of heat transfer enhancement induced by the metal foam, the pure octadecane core (without metal foam) sample with same dimensions, i.e. 196.1576mm by 56.6258mm, is analyzed in Section 3.1 for comparison. Then, Section 3.2 presents the results of the PCM/FOAM system. Besides, two key points, Point A and B as shown in Figure 2, are chosen to investigate the temperature variation in terms of time.

In addition, in the following study, the melting region of the PCM is illustrated by different colour range: the red colour means the temperature exceeding the melting temperature and the PCM has molten to liquid state; the yellow colour represents the temperature around the melting temperature, that is, the PCM is in melting state; the blue colour denotes the temperature is lower than the melting temperature and the PCM keeps the solid state.

3.1 HEAT TRANSFER IN THE PURE PCM

Firstly, the pure PCM is considered for the purpose of comparison. The computational domain is modelled with extra fine mesh scheme consisting of 1832 elements (see Figure 4). From the numerical results shown in Figure 5 it is found that the temperature at Point A, which is close to the heating source, quickly increases from the initial temperature 293K and the PCM at Point A begins to melt at around t=30s at which the temperature approximately reaches the melting temperature 303K. Due to the reason that the PCM has a low thermal conductivity, the heat provided can't be transferred faster and just accumulates around the Point A to make the local temperature increase quickly. At about t=180s, the octadecane has completely changed into liquid state. After this, the temperature begins to increase faster again due to the heat conduction in the liquid. While at Point B, which is far away from the heating surface, there appears a different phenomenon. The temperature at this point slowly increases from the initial temperature 293K and only reaches 300K at about t=6000s. The PCM at the point B changes fully into fluid state until t=12800s. After this, the fast increase of temperature is mainly caused by the heat conduction of the liquid PCM. Figure 6 clearly indicates the variation of the melting front of the PCM in terms of time in the entire domain. It's found that the melting front of the PCM gradually moves upwards as the time increases and keeps almost horizontally at each time instance.

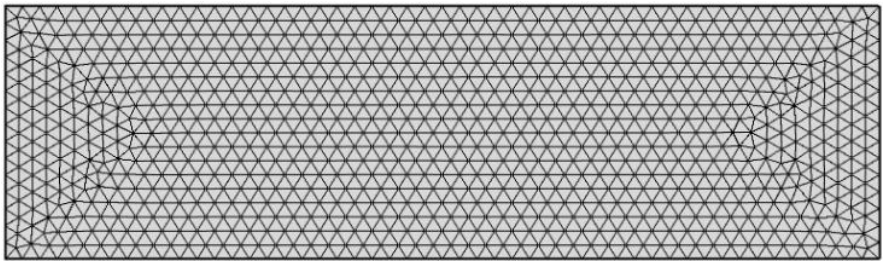

Figure 4. Mesh division for the case of pure PCM

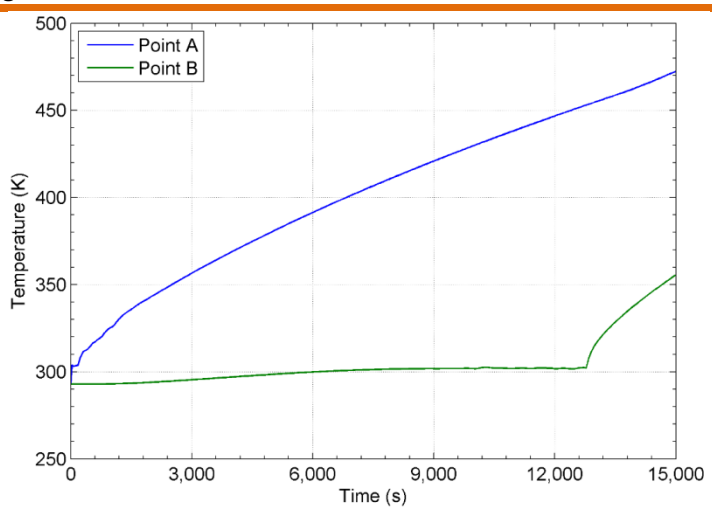

Figure 5. Temperature variation with time for the pure PCM system

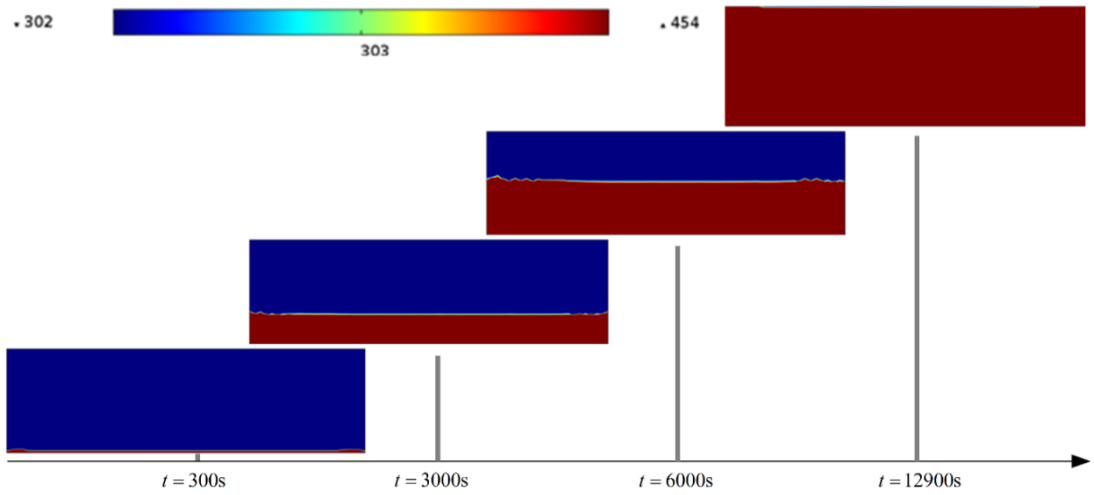

Figure 6. Melting region in the pure PCM system at different time instances

3.2 Heat transfer in the PCM/FOAM system

The computation is carried with the mesh consisting of 428626 elements as shown in Figure 7. Figure 8 displays the variation of temperature at point in the time domain. It is seen from Figure 8 that the PCM octadecane begins to melt at around t=1000s. The temperature at Point A increases more slowly and is obviously lower than that for the case of pure PCM. This is due to the large difference of the thermal conductivity of the metal material and the PCM, thus the heat provided is quickly transferred into the PCM through the metal foam wall and can't accumulate around Point A. Then, in each cell the distributed heat is used for overcoming the latent heat of fusion of the embedded PCM to make it change its phase from the solid state to the liquid state. While at the point B, the temperature increases quickly to almost 303K at t=1200s. After this time, the temperature almost keeps unchanged until at about t=6660s. This is also attributed to the higher thermal conductivity of the metal foam. Then the heat is used for phase change in the cell not for sensible heat increasing. Next, the entire PCM in each cell fully becomes liquid state at around t=7000s. Figure 9 displays the location of the melting front surface of the PCM at different time instance in the PCM/FOAM system. Because of the structure of metal foam, it's found that the melting front surface of the PCM moves upwards but doesn't keep horizontally. The phase change occurs from the outmost to the innermost at each pore.

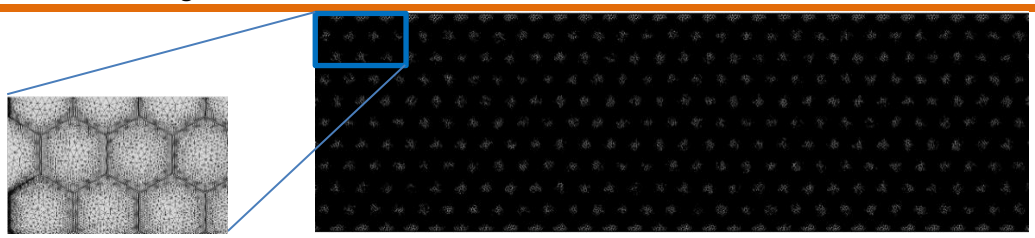

Figure 7. Mesh division of the PCM/FOAM system

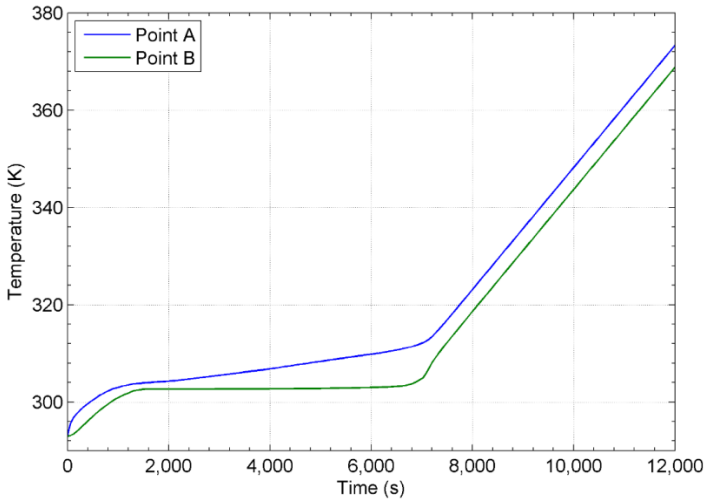

Figure 8. Temperature variation with time for the PCM/FOAM system

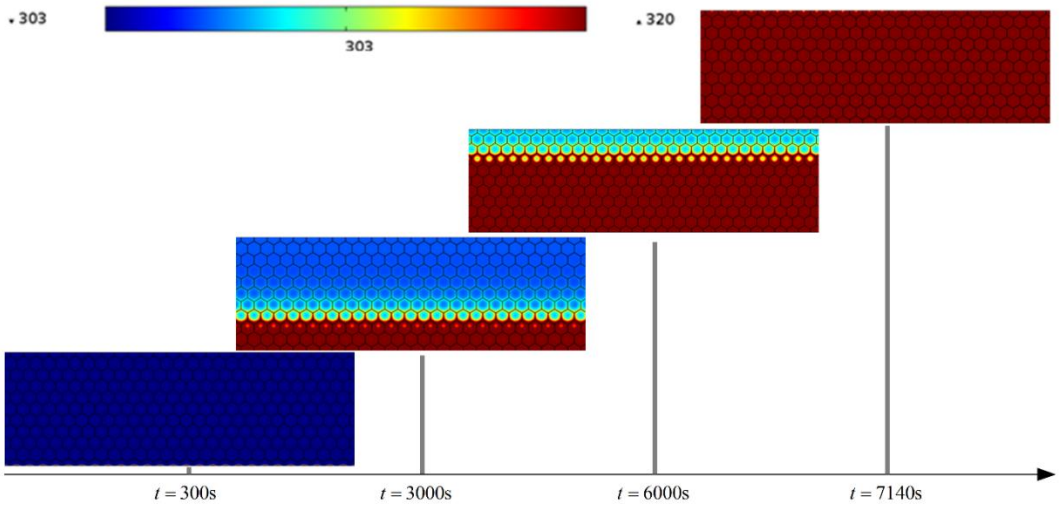

Figure 9. Melting region in the PCM/FOAM system at different time instances

In order to investigate the thermal response at other points different to the particular Point A and B, we chose the middle point or the point very close to the middle point on the top surface as the new check-point C, as displayed in Figure 2. From results in Figure 10, it is observed that there is a slight difference of the temperature variation at the points B and C for both the pure PCM and the PCM/FOAM composite system. For the case of pure PCM, the melting duration of octadecane at the middle point C is slightly later than that at the corner point B, and it is found that the temperature curve at the middle point C is smoother than that at the corner point B. While, for the PCM/FOAM system, the metal foam makes the temperature more uniform and the smaller temperature difference is observed at Point C and Point B.

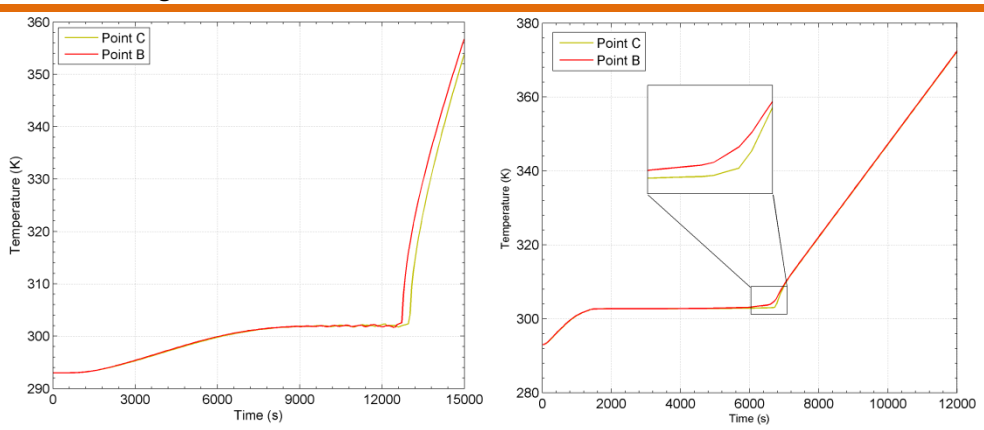

(a) (b)

Figure 10. Temperature variations with time at Points B and C on the top surface for (a) the pure PCM; (b) the PCM/FOAM system

3.3 Sensitivity analysis of thermal conductivity of metal matrix material

As an enhancer, the regular aluminium metal foam has been applied to accelerate the melting of the octadecane. From the viewpoint of composite, both the microstructure of metal foam and the thermal conductivity of metal matrix material are important for the enhanced heat transfer in the PCM. Here, the effect of thermal conductivity of metal matrix material is investigated using different materials. Three typical metal materials including pure iron [22], aluminium [11] and pure copper [22] are taken into consideration and the corresponding thermophysical parameters are listed in Table 2, from which it is found that the thermal conductivity of the three metal materials covers a large range from several tens to several hundreds. Among them, the copper has the highest thermal conductivity, while the iron has the smallest one.

Figures 11 and 12 show the results of the temperature variations with time at Point A and Point B, respectively. From Figure 11 it is found that the temperature at Point A unexceptionally increases with time, among which there is a fastest increase for the case of iron. The main reason is that the iron has far smaller thermal conductivity than the aluminium and the cooper, hence for the case of iron, the input heat energy can't transfer into the PCM rapidly through the metal frame and causes more obvious local heating effect around Point A. At Point B, the temperature distributions in Figure 12 clearly show that the liquid content of the octadecane increases with time. The temperature distributions level out around the melting point (303K), because not all of the energy is going toward a temperature rise and some is being absorbed to change the PCM phase from the solid state to the liquid state. After the PCM is fully liquefied, the temperature increases again because of heat conduction in the liquid PCM. Additionally, the solution in Figure 12 shows that the copper produces the fastest increase of temperature at Point B due to the highest thermal conductivity and thus the phase change of the PCM finishes at first.

Figure 13 presents the melting region at t=6000s in the PCM/FOAM system, which is illustrated by different colour ranges. It's clearly shown that the cooper causes the fastest melting velocity of PCM, due to the huge advantage of its thermal conductivity. This can also be demonstrated by the melting time for the PCM/FOAM system. The PCM/FOAM system can fully melt at about 7440s, 7140s, and 6720s for iron, aluminium and copper matrix materials, respectively. Obviously, the melting time for the aluminium and copper matrix materials reduces approximate 4% and 9.7%, respectively, compared to the iron matrix material.

Table 2. Thermophysical properties of several typical metal materials

Property	Iron	Aluminium	Copper
Density ρ (kg/m^3)	7897	2675	8954
Mass heat capacity c_p $(J/kg/K)$	447	903	384
Thermal conductivity $k(W/m/K)$	80	211	398

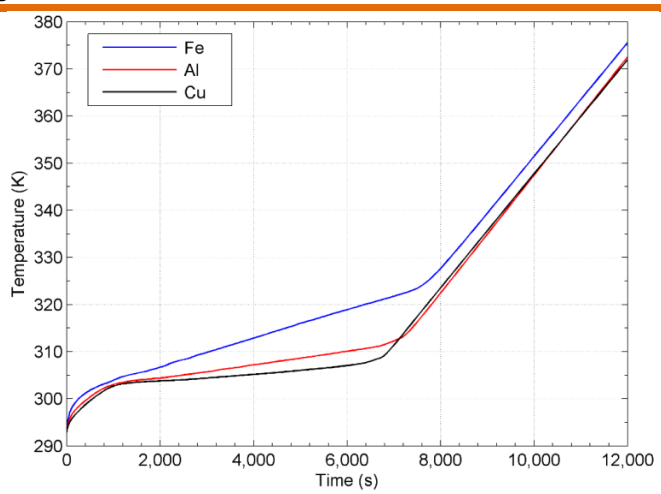

Figure 11. Temperature variations with time at Point A for different metal materials

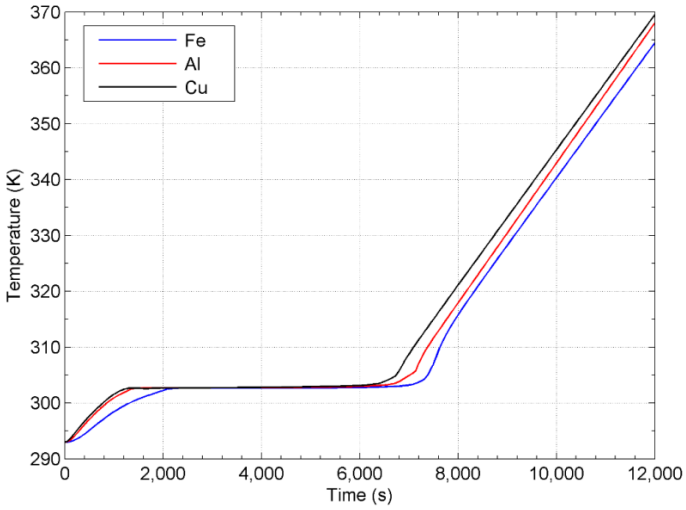

Figure 12. Temperature variations with time at Point B for different metal materials

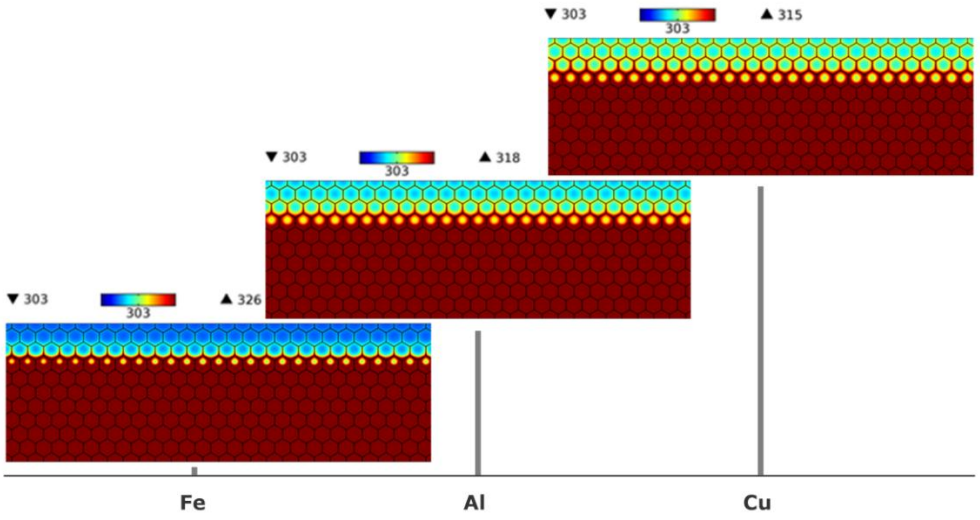

Figure 13. Melting region of the octadecane at $t = 6000$s for different metal matrix materials

3.4 Sensitivity analysis of different PCMs

Apart from the octadecane [10] studied above, there are other PCMs like paraffin series used commonly in engineering applications. Here, the paraffin RT25 [23], RT44HC [7], and RT58 [24] are considered and their results are compared with those of the octadecane with same aluminium matrix material to assess the difference of thermal behaviour between them. Table 3 lists the thermophysical properties of these PCMs. It is seen that the four PCMs have almost the same thermal conductivity. The octadecane and the paraffin RT25 have similar melting temperature, but there is a significant difference of the latent heat of fusion of them. Besides, the paraffin RT58 has the highest melting point, but its latent heat of fusion is relatively small. The paraffin RT44HC has the largest value of latent heat of fusion among the four PCMs.

Figures 14 and 15 present the temperature distributions with time at Points A and B, respectively. Similarly, Figure 14 shows the apparent temperature increase with time at Point A. Figure 15 displays the obvious horizontal level of temperature at the time between 4000s and 12000s, similar to those observed from Figures 11 and 12. But, due to the difference of melting temperature and latent heat of fusion, the four PCMs show different thermal behaviours. Besides, it can be observed from Figure 15 that the length of horizontal level corresponds to the latent heat of fusion of PCM. The smaller the latent heat of fusion is, the shorter the horizontal level is. Also, we find that the location of horizontal level is dependent of the melting temperature. The smaller the melting temperature is, the lower the horizontal level is, and the earlier the melting begins. Finally, Figure 16 displays the melting regions at t=6000s for different PCMs. It is found that the melting region is with respect to the melting temperature and the latent heat of fusion. RT58 corresponds to the smallest liquid content, due to its highest melting temperature. The octadecane and RT25 have similar melting temperature which is significantly lower than that of RT44HC and RT58; thus, the melting starts earlier in the octadecane and RT25. Moreover, we find that the octadecane has larger molten zone than the RT25. It's reasonable that the octadecane has smaller latent heat of fusion than the RT25, so that the melting of the octadecane needs less energy than the RT25. Finally, the full melting times of the four PCMs (the octadecane, RT25, RT44HC and RT58) are 7140s, 11880s, 16260s and 13500s , respectively. Obviously, this result is consistent with that in Figure 15.

Table 3. Thermophysical properties of different PCMs

Property		Octadecane	Paraffin RT25	Paraffin RT44HC	Paraffin RT58
Density ρ (kg/m^3)	Solid	800	785	810	900
	Liquid	800	749	810	760
Mass heat capacity c_p $(J/kg/K)$	Solid	1250	1800	2250	1800
	Liquid	1250	2400	2250	2400
Thermal conductivity k $(W/m/K)$	Solid	0.2	0.19	0.2	0.2
	Liquid	0.2	0.18	0.2	0.2
Latent heat of fusion L_f (J/kg)		125000	232000	270700	179000
Melting temperature T_m (K)		303	300	315	331

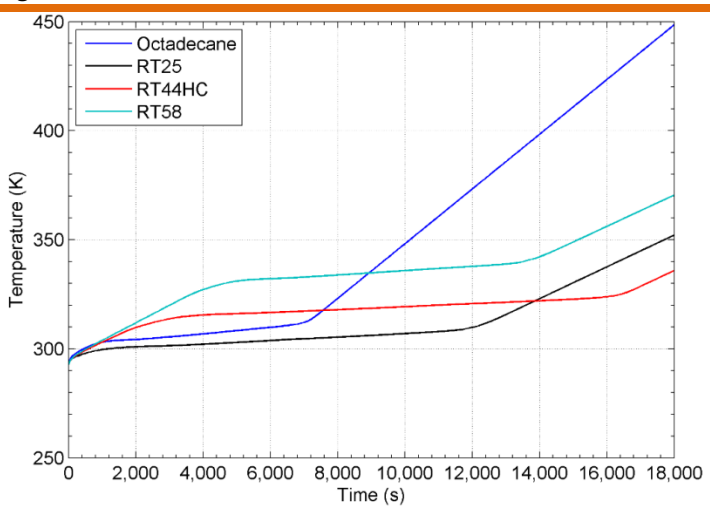

Figure 14. Temperature variations with time at Point A for different PCMs

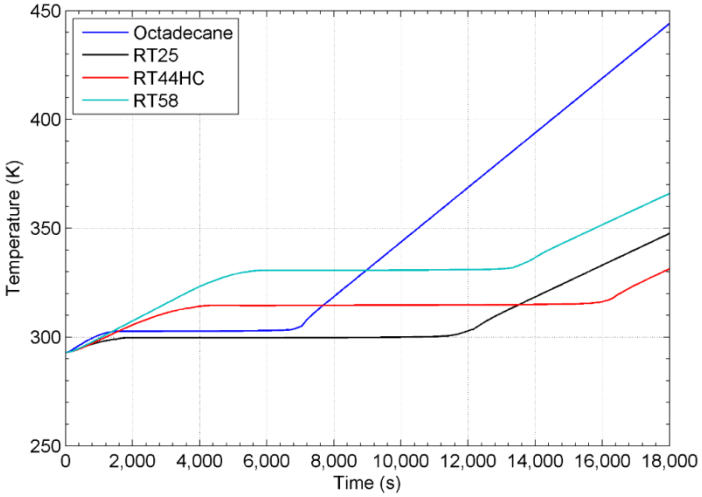

Figure 15. Temperature variations with time at Point B for different PCMs

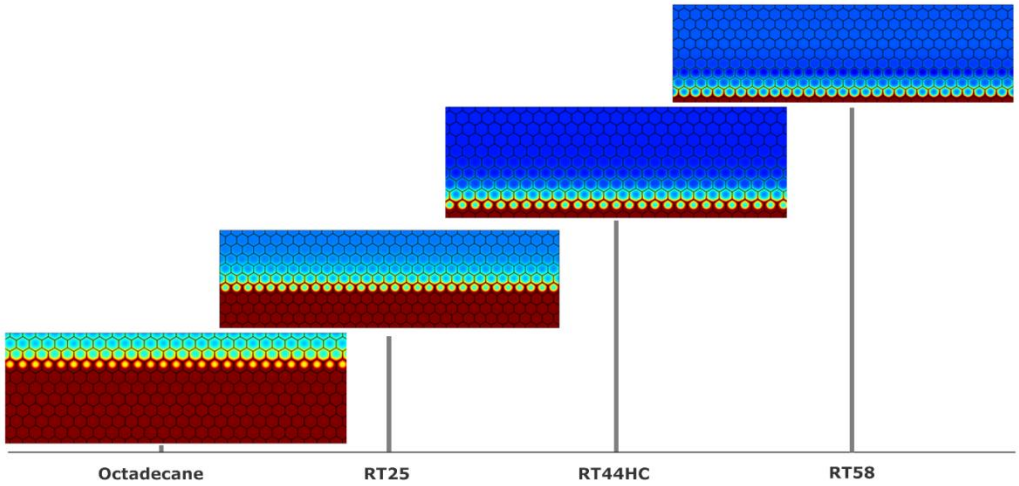

Figure 16. Melting region at $t = 6000$s for different PCMs

3.5 Influence of specific temperature condition

In order to investigate the thermal response caused by specific constant temperature constraint, we applied the constant temperature boundary condition on the bottom surface of the pure PCM domain and the PCM/FOAM domain to replace the given heat flux condition. It is assumed that the specific temperature is 360K, and the corresponding temperature variation in terms of time at Point B on the top surface is recorded. Results in Figure 17 clearly indicate that the addition of aluminium foam makes the temperature at Point B increase rapidly, until the PCM at Point B begins to melt. The heat storage procedure during phase change just finishes at about 30s. Then, the temperature increases continuously and reaches 360K at about 2000s. While, for the pure PCM which has very low thermal conductivity, the poor behavior of heat transfer in it is observed and the PCM needs more time (about 8000s) to finish the phase change. At about 16400s, the PCM fully changes to liquid state.

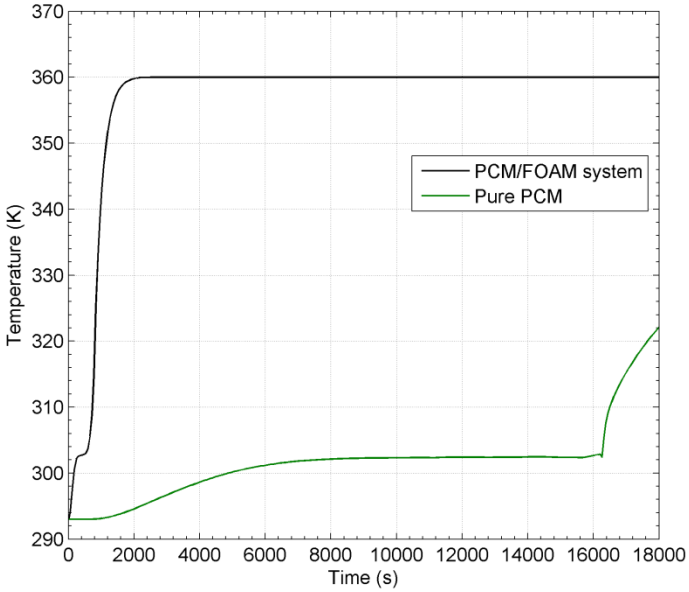

Figure 17. Temperature variations at Point B for the cases of pure PCM and PCM/FOAM system

4. CONCLUSIONS

In this paper, the influence of heat transfer enhancement is numerically studied in the PCM/FOAM system, in which the PCM is enclosed into the pores of the metal foam. Compared to the results of the pure PCM sample, the effect of metal foam on solid/liquid phase change heat transfer is very significant. The huge difference in thermal conductivity between the metal matrix material and the PCM reduces the heat transfer resistance, makes the heat quickly transfer into the local PCM through the metal form and effectively improves the internal heat transfer uniformity of the local PCM. As a result, the melting rate of the PCM can be enhanced by almost 100% by introducing the metal foam. The time of fully melting decreases from about 12800s for the pure PCM system to about 7000s for the PCM/FOAM system. Additionally, the numerical results show that the copper and aluminium matrix materials can reduce 9.7% and 4% melting time, compared to the iron material. Moreover, the octadecane has the shortest melting time compared to the other three PCMs, due to its lower melting temperature and smaller latent heat of fusion. Besides, the thermal response at specific constant temperature condition is investigated and it is found that the metal foam shows stronger advantage to accelerate the phase change (from solid to liquid) of PCM, compared to the case of pure PCM.

Acknowledgements: The work presented in this paper was supported by the open research project by State Key Laboratory of Structural Analysis for Industrial Equipment, Dalian University of Technology, China (Grant No. GZ1610).

REFERENCES

1. Pielichowska, K.; Pielichowski, K. Phase change materials for thermal energy storage. Progress in materials science 2014, 65, 67-123.
2. Ling, T.C.; Poon, C.S. Use of phase change materials for thermal energy storage in concrete: An overview. Construction and Building Materials 2013, 46, 55-62.
3. Mettawee, E.B.S.; Assassa, G.M.R. Thermal conductivity enhancement in a latent heat storage system. Solar Energy 2007, 81, 839-845.

4. Marín, J.M.; Zalba, B.; Cabeza, L.F.; Mehling, H. Improvement of a thermal energy storage using plates with paraffin–graphite composite. International Journal of Heat and Mass Transfer 2005, 48, 2561-2570.
5. Sarı, A.; Karaipekli, A. Thermal conductivity and latent heat thermal energy storage characteristics of paraffin/expanded graphite composite as phase change material. Applied Thermal Engineering 2007, 27, 1271-1277.
6. Ji, H.X.; Sellan, D.P.; Pettes, M.T.; Kong, X.H.; Ji, J.Y.; Shi, L.; Ruoff, R.S. Enhanced thermal conductivity of phase change materials with ultrathin-graphite foams for thermal energy storage. Energy & Environmental Science 2014, 7, 1185-1192.
7. Li, W.; Qu, Z.; He, Y.; Tao, Y. Experimental study of a passive thermal management system for high-powered lithium ion batteries using porous metal foam saturated with phase change materials. Journal of Power Sources 2014, 255, 9-15.
8. Qu, Z.; Li, W.; Tao, W. Numerical model of the passive thermal management system for high-power lithium ion battery by using porous metal foam saturated with phase change material. International Journal of Hydrogen Energy 2014, 39, 3904-3913.
9. Zhao, C.Y.; Lu, W.; Tian, Y. Heat transfer enhancement for thermal energy storage using metal foams embedded within phase change materials (pcms). Solar energy 2010, 84, 1402-1412.
10. Bertrand, O.; Binet, B.; Combeau, H.; Couturier, S.; Delannoy, Y.; Gobin, D.; Lacroix, M.; Le Quéré, P.; Médale, M.; Mencinger, J. Melting driven by natural convection a comparison exercise: First results. International Journal of Thermal sciences 1999, 38, 5-26.
11. Rohsenow, W.M.; Hartnett, J.P.; Cho, Y.I. Handbook of heat transfer. McGraw-Hill: New York, 1998.
12. Qin, Q.H. General solutions for thermopiezoelectrics with various holes under thermal loading. International Journal of Solids and Structures 2000, 37, 5561-5578.
13. Qin, Q.H.; Mai, Y. Crack growth prediction of an inclined crack in a half-plane thermopiezoelectric solid. Theoretical and Applied Fracture Mechanics 1997, 26, 185-191.
14. Qin, Q.H.; Mai, Y.-W. A closed crack tip model for interface cracks in thermopiezoelectric materials. International Journal of Solids and Structures 1999, 36, 2463-2479.
15. Yu, S.; Qin, Q.H. Damage analysis of thermopiezoelectric properties: Part ii. Effective crack model. Theoretical and Applied Fracture Mechanics 1996, 25, 279-288.
16. Qin, Q.-H.; Mai, Y.-W.; Yu, S.-W. Some problems in plane thermopiezoelectric materials with holes. International journal of solids and structures 1999, 36, 427-439.
17. Qin, Q.H. Hybrid trefftz finite-element approach for plate bending on an elastic foundation. Applied Mathematical Modelling 1994, 18, 334-339.
18. Dhanasekar, M.; Han, J.; Qin, Q.H. A hybrid-trefftz element containing an elliptic hole. Finite Elements in Analysis and Design 2006, 42, 1314-1323.
19. Deng, D.W.; Jiang, Y.L.; Liang, D. High-order finite difference methods for a second order dual-phase-lagging models of microscale heat transfer. Applied Mathematics and Computation 2017, 309, 31-48.
20. Takeuchi, Y.; Yoshimoto, Y.; Suda, R. Second order accuracy finite difference methods for space-fractional partial differential equations. Journal of Computational and Applied Mathematics 2017, 320, 101-119.
21. Qin, Q.H.; Mai, Y.-W. Bem for crack-hole problems in thermopiezoelectric materials. Engineering Fracture Mechanics 2002, 69, 577-588.
22. Lienhard IV, J.H.; Lienhard V, J.H. A heat transfer textbook. 3th ed.; Phlogiston Press: Cambridge, 2000.
23. Huang, M.; Eames, P.; Norton, B. Thermal regulation of building-integrated photovoltaics using phase change materials. International Journal of heat and mass transfer 2004, 47, 2715-2733.
24. Agyenim, F.; Hewitt, N. Experimental investigation and improvement in heat transfer of paraffin pcm rt58 storage system to take advantage of low peak tariff rates for heat pump applications. International Journal of Low-Carbon Technologies 2013, 8, 260-270.

Authors

Hui Wang received his Bachelor degree in Theoretical and Applied Mechanics from Lanzhou University, China in 1999. He earned his Master degree from Dalian University of Technology in 2004 and Doctoral degree from Tianjin University in 2007, both of which are in Solid Mechanics. Since 2007, he has worked at Department of Engineering Mechanics, Henan University of Technology. He was promoted to Professor in 2014. His main research interest is in computational mechanics and composite micromechanics, and so far has published more than 50 journal papers and three books respectively by CRC Press and Tsinghua University Press. In 2010, He was awarded the Australia Endeavour Award.

Qing-Hua Qin received his Bachelor of Engineering degree in mechanical engineering from Chang An University, China, in 1982, and his Master of Science and PhD degrees from Huazhong University of Science and Technology (HUST), China, in 1984 and 1990, respectively. Both MS and PhD are in applied mechanics. He joined the HUST Department of Mechanics as an associate lecturer in 1984, and was **promoted** to lecturer of mechanics in 1987 during his PhD candidature period. After spending ten years lecturing at HUST, he was awarded a DAAD/K.C. Wong research fellowship in 1994, which enabled him to work at the University of Stuttgart in Germany for nine months. In 1995 he left HUST to take up a postdoctoral research fellowship at Tsinghua University, China, where he worked until 1997. He was awarded a Queen Elizabeth II fellowship in 1997 and a Professorial fellowship in 2002 at University of Sydney and stayed there till December 2003, both by the Australian Research Council. He is currently working as a professor in the Research School of Engineering at the Australian National University, Australia. He was appointed a guest professor at HUST in 2000 and was a recipient of the J.G. Russell Award from the Australian Academy of Science. He has published over 300 journal papers and six monographs.